

On the potentially dramatic history of the super-Earth ρ 55 Cancri e

Bradley M. S. Hansen^{1*} & Jonathon Zink^{1,2}

¹*Department of Physics & Astronomy, University of California Los Angeles, Los Angeles, CA 90095*

²*Department of Physics & Astronomy, California State University, Northridge, Los Angeles, CA, 91330*

submitted April 2014

ABSTRACT

We demonstrate that tidal evolution of the inner planet (‘e’) of the system orbiting the star ρ 55 Cancri could have led to passage through two secular resonances with other planets in the system. The consequence of this evolution is excitation of both the planetary eccentricity and inclination relative to the original orbital plane. The large mass ratio between the innermost planet and the others means that these excitations can be of substantial amplitude and can have dramatic consequences for the system organisation. Such evolution can potentially explain the large observed mutual inclination between the innermost and outermost planets in the system, and implies that tidal heating could have substantially modified the structure of planet e, and possibly reduced its mass by Roche lobe overflow. Similar inner secular resonances may be found in many multiple planet systems and suggest that many of the innermost planets in these systems could have suffered similar evolutions.

Key words: planet-star interactions – planets and satellites: dynamical evolution and stability

1 INTRODUCTION

The importance of secular gravitational interactions in sculpting planetary systems has long been appreciated as being necessary to understand the regularities of our own solar system. It is known that the long term stability of the terrestrial planets of our solar system is imperilled by the influence of secular gravitational interactions between Mercury, Venus and Jupiter (Laskar 1994; Batygin & Laughlin 2008; Laskar & Gastineau 2009). With the discovery of a host of extrasolar planet systems over the past twenty years, including many multiple systems (Wright et al. 2009; Lissauer et al. 2011a; Fabrycky et al. 2014), the role of secular interactions in determining the stability and architecture of planetary systems is becoming of ever greater importance.

The planetary system around the star ρ 55 Cancri is of particular importance in this regard. One of the first systems discovered by radial velocities (Butler et al. 1997), it also provided one of the first extrasolar giant planets on orbital scales similar to that of Jupiter (Marcy et al. 2002) and, most recently, the revision of the innermost planet parameters (Dawson & Fabrycky 2010) resulted in the photometric detection of a planetary transit (Winn et al. 2011; Demory et al. 2011) which provides some of the best constraints on

the properties of rocky super-earths (Gillon et al. 2012; Demory et al. 2012). Furthermore, the presence of a Jovian class planet with an orbital period of 14 days (55 Canc b) places this system in the enigmatic class of ‘warm Jupiters’, which don’t fit naturally into the evolutionary paradigms developed to explain the presence of Jovian planets with shorter periods. Finally, reports of a tentative detection of an astrometric signal with the HST Fine Guidance sensor (McArthur et al. 2004) suggest that this planetary system may possess a substantial dispersion in orbital inclinations, with a nominal offset of $37^\circ \pm 7^\circ$ between the outer planet 55 Canc d and the edge-on inner planet 55 Canc e.

It has also been suggested (Kaib, Raymond & Duncan 2011) that the presence of a distant M-dwarf companion (Mugrauer et al. 2006) can induce a coherent precession of the entire planetary system (Innanen et al. 1997), potentially leading to a substantial obliquity offset between the stellar spin and the orbital plane of the planetary system. However, for the 55 Cancri system, spin-orbit coupling between the star and the planets likely quenches such an offset unless the companion is in a highly eccentric ($e \sim 0.95$) orbit (Boue’ & Fabrycky 2014). Observationally, the situation is unclear as Bourrier & Henrard (2014) claim to have detected a projected obliquity of $72 \pm 12^\circ$, which Lopez-Morales et al. (2014) claim is impossible given the very low stellar rotation.

All of this recent activity suggests that the 55 Can-

* E-mail: hansen@astro.ucla.edu

cri system is interesting for both its dynamical architecture and history as well as for the composition of the component planets, in particular 55 Canc e, as an example of a massive, earth-like planet transitting a bright star. Our analysis will focus on the fact that 55 Canc e is close enough to the star that it should have experienced substantial tidal dissipation, and consequent orbital evolution. Such evolution can have an effect on more distant planets too, as secular coupling between the planets can transfer angular momentum back and forth between the planets in the system (e.g. van Laerhoven & Greenberg 2012). In § 2 we will discuss our model for tidal interactions and describe the evolution of the system within the context of classical secular theory, and we will show how this can provide a potential explanation for the large inclination dispersion. In § 3 we investigate the evolution further using numerical integrations, to clarify the dynamical limitations on the excitation of inclination and discuss the influence of the near-resonance of Planets 55 Canc b and 55 Canc c on the secular oscillations of the system. Finally, we discuss the possible influence of tidal heating on the structure of 55 Canc e and on the likelihood of other known planetary systems where inclination excitation could have occurred.

2 TIDAL EVOLUTION IN THE CLASSICAL SECULAR APPROXIMATION

The physical parameters of the innermost planet, 55 Cancri e, are estimated to be a mass of $7.99 \pm 0.25 M_{\oplus}$ and a radius of $2.00 \pm 0.14 R_{\oplus}$ (Nelson et al. 2014; Winn et al. 2011; Demory et al. 2011). The radius of a perovskite planet of this mass is $\sim 1.9 R_{\oplus}$, using the fitting formulae of Seager et al. (2007). Thus, although it is closer in mass to a Neptune or Uranus, this is expected to be a predominantly rocky planet (although it could have a finite water contribution as well). We wish to therefore consider a range of tidal dissipation extending from terrestrial values to ice giant values.

To implement the tidal dissipation within the secular formalism, we use the same approach as in Hansen & Murray (2014), following on from prior work of Wu & Goldreich (2002) and Greenberg & van Laerhoven (2011). We have also previously examined tidal dissipation for extrasolar giant gas planets (Hansen 2010), using the formalism of Hut (1981) and Eggleton et al. (1998). However, the restriction of classical secular theory to the quadratic level in eccentricity means that we will restrict our tidal expressions to the same order. We must also choose a dissipation level more appropriate to terrestrial planets. Choosing a bulk dissipation constant that yields $Q' = 10$ for the Earth (e.g. Goldreich & Soter 1966), we find

$$\frac{d \ln a}{dt} = \frac{e^2}{25 \text{ Myr}} \left(\frac{a}{0.1 \text{ AU}} \right)^{-8} \left(\frac{R_p}{2R_{\oplus}} \right)^{10} \frac{8M_{\oplus}}{M_p} \quad (1)$$

$$\frac{d \ln e}{dt} = \frac{1}{50 \text{ Myr}} \left(\frac{a}{0.1 \text{ AU}} \right)^{-8} \left(\frac{R_p}{2R_{\oplus}} \right)^{10} \frac{8M_{\oplus}}{M_p}. \quad (2)$$

We have included the estimated mass and radius for 55 Canc e in these estimates, but let the semi-major axis float. This demonstrates that we expect substantial tidal evolution for a planet like this even out beyond 0.1 AU,

unless the strength of the dissipation is several orders of magnitude weaker than expected.

Of course, there is little evolution if the orbit starts close to circular, but the presence of much larger planets in close proximity suggests that a finite eccentricity would be excited by secular perturbations anyway, resulting in tidal evolution (e.g. Mardling & Lin 2004). Thus, we need to consider the fact that the currently observed configuration could be the result of substantial tidal migration if we wish to infer something about the origin and evolution of this planetary system.

2.1 Secular Architecture

Consider then the classical secular solution for the 55 Cancri system with the currently measured parameters of Nelson et al. (2014). In addition to the classical equations to second order in eccentricity and inclination (Murray & Dermott 1999), we also include the effects of relativistic precession (Adams & Laughlin 2006). There is potentially also an additional precession due to the presence of a distant M dwarf companion, a $0.26 M_{\odot}$ M dwarf located at 1260 AU (Mugrauer et al. 2006). However, this is too small to affect the dynamics of the planetary configuration on small scales, although it can generate precession of the system as a unit (Innanen et al. 1997; Kaib et al. 2011; Boue' & Fabrycky 2014). In order to better match the observations, we furthermore assume that the planetary system invariable plane is inclined at 37° to the line of sight, except for the transitting 55 Canc e. This increases all the masses by a factor of 1.25 from that inferred in the radial velocity solution. These are summarised in Table 1.

The modal structure for the eigenvalues that results from this configuration is such that the eccentricities of the outer two planets are decoupled from the inner three (as noted by van Laerhoven & Greenberg 2012), whose interaction will dominate the eccentricity of 55 Canc e in the absence of dissipation. On the other hand, all four of the inner planets are coupled to a low frequency inclination eigenmode that represents the precession of the inner system under the influence of the M dwarf perturber and 55 Canc d.

If the inner planet migrated due to tidal dissipation, then the secular structure of the system will have changed as well. Figure 1 shows how the secular eigenfrequencies of this system vary as we vary the semi-major axis of Planet e, keeping all masses and other semi-major axes fixed, from the current location to a semi-major axis of 0.05 AU, corresponding to a period of 4.2 days. The two lowest eigenfrequencies in eccentricity correspond to the outer planets d and f, and do not change because the outer planets are essentially decoupled. The lowest frequency inclination eigenfunction corresponds to a mode coupling the four innermost planets.

The higher frequency eigenmodes show a more interesting structure. In particular, we see that the two highest frequency modes in both inclination and eccentricity experience resonant behaviour in the interval $a_e \sim 0.026$ – 0.031 AU. Thus, if 55 Canc e starts with a semi-major axis exterior to 0.032 AU (orbital period of 2.15 days), it will cross first an inclination resonance and, shortly thereafter, an eccentricity resonance. These will result in mode mixing and can result in interesting behaviour, as we shall see. For

Table 1. Basic Architecture of the 55 Cancri Planetary System, based on the parameters of Nelson et al. (2014) and assuming an inclination of 37° to the line of sight for all but the innermost planet.

Planet	a (AU)	M (M_J)
e	0.035	0.0251
b	0.1134	1.056
c	0.2374	0.223
f	0.774	0.184
d	5.451	4.79

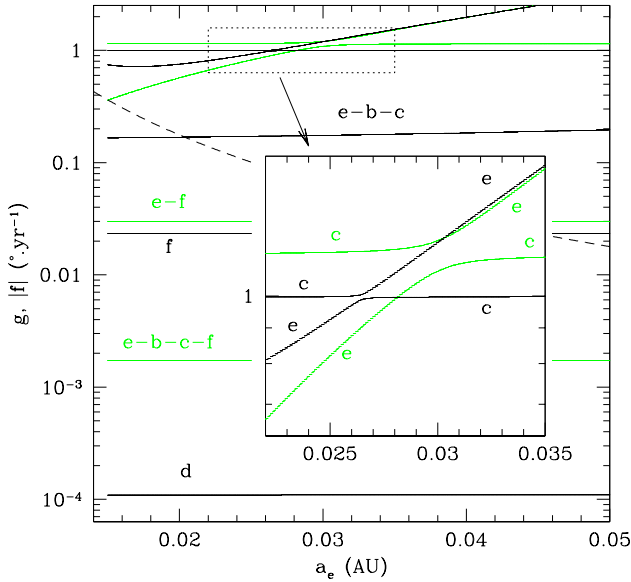


Figure 1. The black curves show how the precession frequencies of the secular eccentricity eigenvalues g_i change as the semi-major axis of 55 Cancri e is varied, with all other semi-major axes and masses held constant. The green curves show the equivalent absolute values of the frequencies for the inclination eigenvalues, $|f|$. The inset shows a zoom around the most interesting part of parameter space. The various curves are labelled with the symbols for all planets that make at least a 10% contribution to the unit eigenvector of that mode. We see that, if 55 Cancri e moves through the region ~ 0.026 – 0.031 AU, the system will experience secular resonances between both eccentricity and inclination eigenmodes. In particular, these highlight that the principal interaction is between 55 Cancri e and 55 Cancri c, not the second most distant 55 Cancri b. However, all three planets interact via a third eccentricity mode, while the outer two planets are essentially decoupled. In the case of the inclinations, the inner four planets also precess as a unit under the influence of the outermost planet. For completeness, the dashed curve shows the value of the relativistic precession frequency at the location of 55 Cancri e.

the purposes of the following discussion, we designate the eccentricity resonance as g_{ce} and the inclination resonance as f_{ce} .

The dashed line in Figure 1 also shows the strength of relativistic precession on these close planetary scales. We have repeated the above calculation without either of the externally imposed precessions and verified that the behaviour is qualitatively similar. The relativistic contribution has two quantitative consequences. The first is that the frequencies of the inclination and eccentricity precessions for 55 Cancri e

are the same on small scales without relativity (the black-green pair labelled e in the inset lie on top of one another for $a_e < 0.026$ AU) and the turnup in the eccentricity eigenfrequency of 55 Cancri e at $a_e < 0.018$ AU is a consequence of relativity.

2.2 Tidal Evolution

Let us now consider the tidal evolution of a 55 Cancri analogue in which 55 Cancri e starts with an original semi-major axis $a_e(0) > 0.04$ AU. The secular coupling of the inner three planets means that the tidal dissipation will remove energy from the system as a whole instead of just 55 Cancri e (Wu & Goldreich 2002; Greenberg & van Laerhoven 2011; Hansen & Murray 2014), and so, the current rather small eccentricities of 55 Cancri b and c may have been substantially damped. We take the eccentricity of 55 Cancri f to represent a primordial value because it is largely decoupled from the inner three planets. Let us start then, for illustrative purposes, with the same eccentricity for planets b, c and f, ~ 0.32 . Figure 2 shows the evolution of the system under the influence of tidal dissipation using equations (1) and (2). The modelling of the interactions between the tides and the secular oscillations is performed using the formalism of Hansen & Murray (2014). Figure 2 shows three sets of curves, for three different levels of dissipation $Q'_e = 10, 100$ and 1000 . We see that the consequence of the resonant crossings is the excitation of inclination and eccentricity for 55 Cancri e. The excitation of the eccentricity also results in a rapid increase in the strength of the tidal dissipation and a sharp decrease in semi-major axis.

The size of the rapid ‘jump’ in semi-major axis is dependant on the strength of dissipation Q'_e , and is larger for weaker dissipation. This is a little counter-intuitive but can be understood in terms of the speed at which 55 Cancri e moves through the g_{ce} resonance. The origin of the high eccentricity of 55 Cancri e is the mixing of the two mode amplitudes during the g_{ce} passage, and a slower passage results in a larger transfer of amplitude between the two modes. The higher eccentricity means a smaller periastron and more inward migration.

The increase in inclination i_e seen in Figure 2 offers an explanation for the curious misalignments of 55 Cancri e and d. If 55 Cancri e began in the same disk plane as d and all the other planets, but migrated inwards through the secular resonances, then inclination offsets $\sim 20^\circ$ or greater are quite plausible.

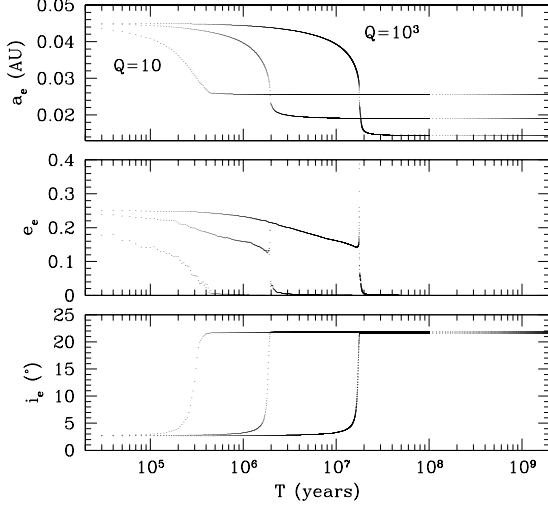


Figure 2. The upper panel shows the temporal evolution of the semi-major axis of 55 Canc e as the planetary system evolves under the influence of tides and secular coupling. We show the evolution for three values of $Q'_e = 10, 100$ and 1000 . We see that weaker dissipation actually leads to more orbital migration. The reason for this counter-intuitive behaviour can be found in the middle panel, which shows that the eccentricity excitation during the resonant crossing is stronger if the tidal dissipation is weaker. The lower panel shows the increase in the planetary inclination due to the crossing of the inclination resonance.

2.3 Analytic Estimates

Minton & Malhotra (2011) have investigated the excitation of eccentricity in solar system asteroids by sweeping secular resonances driven by outer planet migration. This formalism can be adapted to understand the excitation of eccentricity and inclination in the 55 Cancri system too. One important difference is that the interaction discussed in MM11 is driven by the change in the frequency of the external resonance, whereas the interaction here is driven by the inward drift of the excited body, as it crosses a fixed external resonance. In appendix A we discuss the MM11 analysis, demonstrate that the end result is similar despite the modification to the model, and present the equivalent expression for the inclination. Here we will briefly review the outline of those results.

MM11 start with a Hamiltonian of the form

$$H_e = -g_0 J + \epsilon \sqrt{2J} \cos(\bar{\omega}_p - \bar{\omega}) \quad (3)$$

where $J = \sqrt{a}(1 - \sqrt{1 - e^2})$, g_0 is the precession frequency for the longitude of periastron $\bar{\omega}$, and ϵ parameterises the strength of the coupling to the externally maintained secular mode, whose orientation is $\bar{\omega}_p$. To this Hamiltonian, we add the terms that describe the corresponding interaction for the inclination

$$H_i = -h_0 Z + \delta \sqrt{2Z} \cos(\Omega_p - \Omega) \quad (4)$$

and $Z = \sqrt{a(1 - e^2)}(1 - \cos i)$.

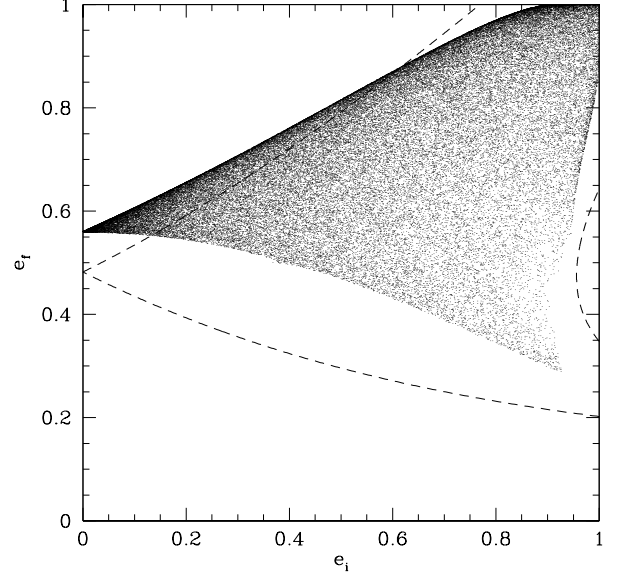


Figure 3. The dashed lines enclose the range of possible final eccentricities, depending on initial eccentricity and longitude of periastron, calculated in the limit of low eccentricity. The points show the solution using the full expression for J , which preserves the basic structure of the low e expansion, but shifts the solution to higher values. These solutions are for the case $e_b = 0.1$, and will shift according to this quantity and the strength of the tidal dissipation.

For the size of the eccentricity jump from J_i to J_f , they derive

$$J_f = J_i + \frac{\pi \epsilon^2}{2|g_0|} + \epsilon \sqrt{\frac{2\pi J_i}{|g_0|}} \cos \bar{\omega}_i. \quad (5)$$

The size of the jump is thus regulated by the rate of change of g_0 due to tidal dissipation, as seen in the previous section, as well as the phase of the pericenter precession, $\bar{\omega}_i$. The expression for this is

$$\dot{g}_0 = \frac{n}{8a} \left(\sum_j \frac{m_j}{m_c} \alpha_j^2 \gamma_j - \frac{15}{2} \frac{GM_c}{c^2 a} \right), \quad (6)$$

where n is the orbital frequency, $\alpha_j = a/a_j$ is the ratio of semi-major axes of 55 Canc e and perturber j , $\gamma_j = b_{3/2}^{(1)} + 3\alpha_j [b_{5/2}^{(0)} - 2\alpha b_{5/2}^{(1)} + b_{5/2}^{(2)}]$ and the functions $b_s^{(i)}$ are the Lagrange functions (functions of α_j).

Taking \dot{a}/a from equation (1) we see that the rate of dissipation actually depends on the eccentricity, which is the quantity being excited during the transition. Thus, the speed at which the planet crosses the resonance accelerates as the eccentricity is excited – a naturally self-limiting process. To estimate the final eccentricity, we thus express $\dot{g}_0 = e_f^2 g_0 / \tau_0$, where e_f is the final eccentricity. In the limit of low eccentricity, $J \sim \frac{1}{2} \sqrt{a} e^2$, so that the final expression is

$$e_f^2 \sim e_i^2 + \frac{\pi \epsilon^2 \tau_0}{2g_0 \sqrt{a} e_f^2} + \epsilon \sqrt{\frac{2\pi \tau_0}{g_0 \sqrt{a}}} \frac{e_i \cos \bar{\omega}}{e_f}. \quad (7)$$

The size of the eccentricity jump is large enough, however, that we should use the full expression for J_f . Figure 3

shows the resulting range of final eccentricities as a function of initial eccentricity, for our nominal $Q'_e \sim 10$, assuming $e_b = 0.1$. We can see that, for small initial eccentricities, there is a unique final eccentricity ~ 0.56 , although this will, of course, be damped further by tidal evolution after the resonance has been crossed. In the absence of further eccentricity excitation, this also predicts a final semi-major axis $\sim a_0(1 - e_f^2) \sim 0.0205\text{AU}$, for $a_0 = 0.03\text{ AU}$. The size of the eccentricity jump also scales with the eccentricity of 55 Canc b. If e_b is as small as 0.01, then the final eccentricity is ~ 0.18 in the limit of low initial eccentricity. Nevertheless, we see that substantial eccentricities can be generated even if the eccentricity of the perturbing planets are relatively small. The eccentricity of Planet b may also experience moderate pumping due to the coupling between planets e, b and c via a third mode (see Figure 1), but this is limited by the large mass ratio.

We find a similar inclination excitation,

$$Z_f = Z_i + \frac{\pi\delta^2}{2|\dot{h}_0|} + \delta\sqrt{\frac{2\pi Z_i}{|\dot{h}_0|}} \cos \Omega_i. \quad (8)$$

Since τ_0 once again depends on the eccentricity, we note that the inclination resonance lies slightly outside the eccentricity resonance, so that we expect this to scale with e_i , not e_f . In the limit of low eccentricity and inclination, the analogue to equation (7) is

$$i_f^2 = i_i^2 + \frac{\pi\delta^2\tau_0}{2h_0\sqrt{ae_i^2}} + \delta\sqrt{\frac{2\pi\tau_0}{h_0\sqrt{a}}} \frac{i_i}{e_i} \cos \Omega_i. \quad (9)$$

In the limit of low initial eccentricity and inclination, this still predicts a final inclination $\sim 45^\circ$, for values of 55 Canc b of $e_b = 0.1$ and $i_b = 2^\circ$.

Therefore, this analysis supports the idea, expressed in the previous section, that substantial changes in inclination and eccentricity are possible for reasonable planetary parameters. It also demonstrates the dependance on parameters, in that eccentricity and inclination changes increase with the dissipation timescale τ_0 , i.e. crossing the resonance more slowly increases the excitation.

2.4 Additional Planets

The present analysis is based on the secular behaviour of the observed planets. However, the secular oscillations depend on the effects of all the planets in the system, which raises the question whether it is possible to substantially alter the properties of the system evolution if there are as-yet-undetected planets present.

To assess this effect, we have taken the collection of extant radial velocity data from Nelson et al. (2014), Endl et al. (2012) and Fischer et al. (2008) and determined how large a planet could remain undiscovered in this data. The orbital periods of the five known planets were held fixed at the values determined by Nelson et al. but other parameters such as mass, eccentricity and longitude of periastron were allowed to vary, and then the data was refit with a series of models with an additional planet with a range of mass and semi-major axis. Orbital periods from 94 to 3900 days were searched, and the mass constraints were defined as those that would yield a signature larger than a 90% confidence

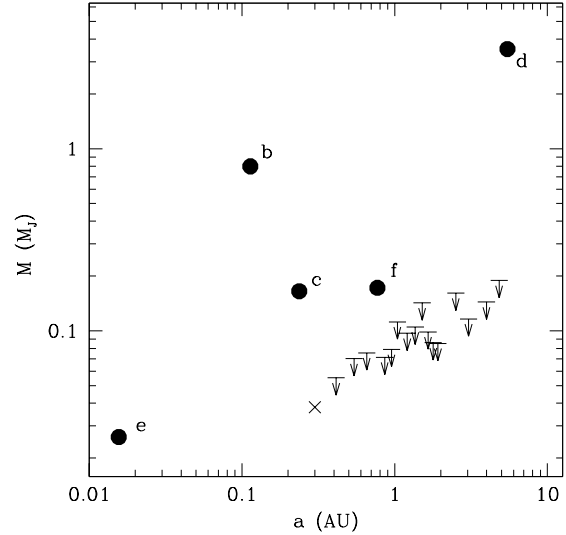


Figure 4. The solid points show the currently known planets of the ρ 55 Cancri system, with the radial velocity values for the masses shown. The upper limits indicate the 90% confidence mass limits for selected regions of period space. Planets with this period and masses larger than this limit should have already been detected in the radial velocity data. The cross shows the approximate location of the tentative 60.76 day signal discussed in passing by Nelson et al. (2014).

level fluctuation with respect to the best fit. The resulting mass limits are shown in Figure 4.

For planets in the range 0.4–0.75 AU, radial velocity signals would be detected for planets with masses $> 4 \times 10^{-5} M_\odot$. If we include a single planet of this mass and period in our secular evolution, it results in no qualitative changes to the evolution. This is because the extra planet only exhibits a substantial coupling to two modes. The first is a mode dominated by the new planet alone, and the second mode is the mode coupling all of the inner planets together (the mode marked e-b-c in Figure 1). Thus, another planet in this gap would share in the mode that mixes all the planets together, and can contribute to the angular momentum budget of the secularly coupled system, but it does not substantially alter the structure of the modes that undergo the g_{ce} and f_{ce} resonant interactions). We have tested the effects of planets an order of magnitude larger than our RV limit and still find no substantial qualitative change in the mode behaviour. Nelson et al (2014) note the presence of a weak signal in their data with period 60.76 days and velocity semi-amplitude $\sim 2\text{m/s}$. This is of similar magnitude to the limits we find, and so, if such a planet exists, it would not substantially change the secular structure of the system.

We have also tested the effects of a planet in the gap between planets f and d. If such a planet improves the secular coupling of the inner planets and the outer planets, it might change the evolution of the system by providing a greater reservoir to store angular momentum and might help to drive an even stronger evolution. However, with mass limits $< 0.1 M_J$, extra planets with $a > 1\text{ AU}$ appear to only

weaken any residual coupling between inner and outer planets. New planets interior to this would be within the 3:2 commensurability with planet f and should provide strong dynamical signatures that would be detected in the radial velocities.

We therefore conclude that the behaviour discussed here is likely to be robust with respect to the presence of as-yet-undetected planets in the 55 Cancri system.

3 NUMERICAL EXPLORATION

The analytic and semi-analytic results offer a qualitative explanation for the possible origin of a large inclination difference in the 55 Cancri system, but there are several reasons to be cautious about the quantitative results. Our initial estimates suggest that eccentricities and inclinations can reach substantial values, exceeding the approximations of classical secular theory. Furthermore, the proximity of planets 55 Canc b and 55 Canc c to the 3:1 mean motion resonance could possibly amend the secular oscillations and shift the resonance locations. This can be incorporated into the classical formalism in the case of first order resonances (Malhotra et al. 1989) but higher order resonances scale with higher powers of eccentricity and inclination, which would introduce nonlinearities into the classical secular equations. Thus, we have performed numerical integrations of model systems with the Mercury6 code (Chambers 1999) to examine the secular structure of actual 55 Cancri analogues.

The standard Mercury6 algorithm does not account for relativistic precession nor tidal evolution of the orbit. We have thus included a central potential contribution to produce the former and account for the latter by instituting a drag force by including a radial velocity damping term. The small stepsizes required to resolve these short period orbits means that we are able to reproduce the expected precession rate without needing to incorporate individual stepsizes (e.g. Saha & Tremaine 1994). We describe the calibration of the latter in appendix B.

3.1 Test Particle Orbits

The simplest test of the effect of the 3:1 resonance is to examine the secular oscillations of test particles interior to 55 Canc b. We simulated several analogues of the 55 Canc planetary system with 55 Canc e replaced by a set of test particles on co-planar circular orbits and with a range of semi-major axes, in order to understand the secular forcing this planet would experience from the other four. We chose the longitudes of periastron and ascending node randomly for the four planets and integrated several cases, to understand what sort of secular behaviours might be expected.

Figure 5 shows the expected result, based on the considerations of § 2. We start with 800 test particles on circular, coplanar orbits between 0.015 and 0.065 AU, perturbed by the four planets of the 55 Cancri system with $a > 0.1$ AU. The figure shows the resulting forced eccentricity and inclination after 1.1 Myr of evolution. Over most of this range, the appearance of simple Lagrange oscillations are evident, but at $a \sim 0.03$ AU, both eccentricity and inclination grow due to the resonance of the free Lagrangian precession of

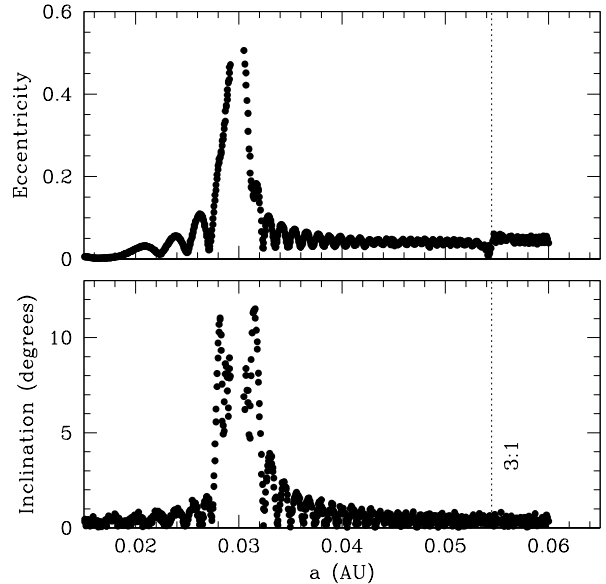


Figure 5. The upper panel shows the eccentricity, while the lower panel shows the inclination, after 1.1 Myr of evolution. Further evolution can drive the eccentricity to high enough values to impact the star.

the test particles with the secular oscillations of the forcing planets.

However, other behaviour is also possible. Figure 6 shows the evolution of the same test particle setup but forced by a planetary system with a different choice of eccentricities and longitudes of periastron and ascending node. In this case the inclination resonance occurs at approximately the same location, but the eccentricity resonance occurs at $a \sim 0.05$ AU. Further examination of the results from this integration shows that the resonant angles generated by the pair 55 Canc b and 55 Canc c circulate most of the time, but undergo intermittent passages through resonance, which occur when the secular oscillations bring one of the planetary eccentricities close to zero. The origin of this behaviour is discussed in more detail in appendix C, but the salient feature for this analysis is that this interaction between resonant and secular behaviour is enough to shift the secular resonance in some cases.

3.2 Tidal Evolution

In order to examine the consequences of this kind of evolution for plausible 55 Cancri origins, we perform the following numerical experiment on the 55 Cancri system, using the Mercury6 code.

We integrated 100 systems with 55 Canc e originally located at 0.033 AU (i.e. just outside the secular resonance location in the classical estimate). The other four planets assume the semi-major axes determined by Nelson et al. (2014) from the latest compilation of the data. We assume masses for the four outer planets assuming an inclination angle of 53° (i.e. an enhancement by a factor of 1.25 above the nominal edge-on estimate), although we retain the nominal mass of 55 Canc e because it is transiting and therefore

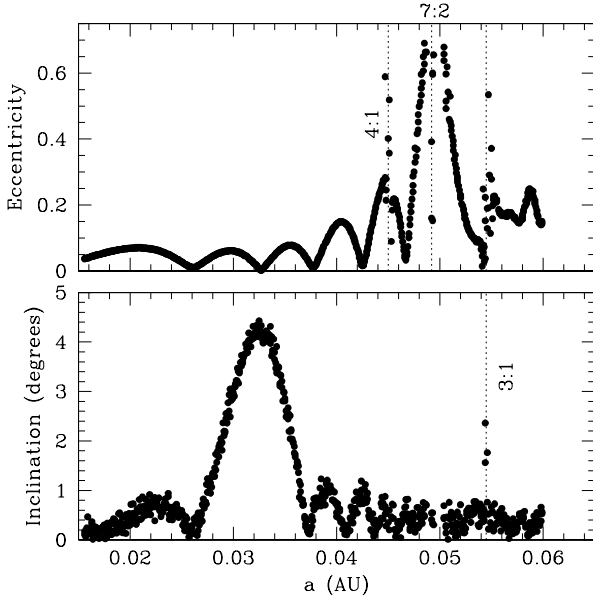


Figure 6. The upper panel shows the eccentricity, while the lower panel shows the inclination, after 0.3 Myr of evolution. In this case we see that perturbations due to the proximity of the 3:1 resonance have shifted the location of the eccentricity resonance without shifting the location of the inclination resonance markedly. The larger eccentricities also lead to enhanced contributions from mean motion resonances with 55 Canc b as well.

has inclination of 90° . Tidal dissipation tends to align the longitudes of pericenter, so we draw the initial longitudes of perihelion and ascending node, as well as the mean longitude at the start, from uniform distributions. The inclinations are chosen from a Gaussian distribution with dispersion of 2° , which is consistent with estimates for the flatness of compact planetary systems based on Kepler studies (Lissauer et al. 2011a; Tremaine & Dong 2012; Fang & Margot 2012). Tremaine & Dong (2012) note that larger inclination dispersions are possible, but our assumption represents a conservative starting point in order to illuminate the size of the effect produced by the secular resonance. Although the 55 Cancri planets have measured eccentricities, these could have been substantially reduced by the effects of tidal damping and secular coupling. In order to assess the strength of the possible interactions, we draw our initial eccentricity distribution from the eccentricities observed in other planetary systems. Several proposals have been made for describing the exoplanet eccentricity distribution (e.g. Shen & Turner 2008) but including planets at large orbital periods and single planets may overestimate the eccentricities for planets in compact multiple systems. Wang & Ford (2011) estimate the eccentricities for single planets with short orbital periods but do not include multiples. Limbach & Turner (2014), on the other hand, derive the eccentricity distribution as a function of multiplicity, but include systems on large scales. We opt to draw our eccentricities from the ‘short period’ beta distribution fit by Kipping (2013) to the observed exoplanet data with orbital periods < 382 days. This draws values from the cumulative probability

$$P(e) = \frac{\Gamma(3.967)}{\Gamma(0.697)\Gamma(3.27)} e^{-0.303} (1-e)^{2.27}. \quad (10)$$

We adopt this as representative of the potential initial conditions in the 55 Cancri system as it includes the bulk of the 55 Cancri planets (except for 55 Canc d) within its period (< 387 days) threshold. The systems are then integrated for 1 Myr. Our implementation of tidal evolution in Mercury6 uses the force law used by Hut (1981), to damp eccentricity. As discussed in appendix B we calibrate the dissipation in order to produce an eccentricity damping timescale of 1.3×10^5 years for an $8M_\oplus$ planet at $a=0.033$ AU. For a planetary radius of $R = 2R_\oplus$, this is equivalent to $Q' = 13$.

Of the 100 planetary systems integrated, 33 underwent dynamical instability, usually after less than 0.1 Myr (where we define this as undergoing planetary scattering and collisions which removed at least one and often several planets from their observed orbits – be it by ejection or collision with the star or another planet). This indicates that even the reduced eccentricities of Kipping’s ‘short period’ distribution are sometimes too large for a system as closely packed as the 55 Cancri system. Of the 67 systems whose planets survive to the present, 38 reach semi-major axes < 0.03 AU within 1 Myr, while 29 do not. Those that pass within 0.03 AU usually lie well inside 0.03 AU, as shown in the right-hand panel of Figure 7. This is a consequence of the eccentricity jump due to the secular resonance and the subsequent circularisation of the orbit. Figure 7 also shows the resulting inclination distribution of the 38 systems with final semi-major axis < 0.03 AU. We find inclinations can be pumped up to almost 60° , in agreement with the simple estimates of earlier sections. It should be noted that the inclinations shown in Figure 7 are the amplitudes of the secular oscillations, not the instantaneous values, which is why the initial conditions (dotted histogram) are larger than the seed distribution (dashed histogram) – the secular forcing from the other planets drives the inclination of 55 Canc e up even if the initial value is small.

Of the 29 stable systems that do not penetrate inside 0.03 AU within 1 Myr, it is possible that some may just have insufficient amplitude in the relevant modes to secularly pump the eccentricity of 55 Canc e to values that promote tidal evolution. However, the distribution of initial eccentricities for 55 Canc b, which is the principal driver of the secular pumping, is quite similar to those cases which do migrate, as shown in Figure 8. This suggests that many of the systems have sufficient amplitude, but have had their eigenvalues shifted enough by the 3:1 resonance that it lies exterior to the starting location of our simulation.

To test this hypothesis, we repeat the integration of 10 of the systems which do not undergo sufficient evolution, with all of the same parameters except that the initial semi-major axis of 55 Canc e is taken to be 0.045 AU instead. This is to place it closer to the region destabilized in the case shown in Figure 6. Of these, two exhibited little evolution, but in another five, 55 Canc e experienced such strong eccentricity excitation that it collided with the star with little semi-major axis evolution or inclination excitation. In the remaining three, the inner planet achieved a 55 Canc e analogue orbit, with a circularised orbit with $a < 0.03$ AU, and maximum inclinations of 8.2 , 12.7 and 18.2° . Thus, in many of these systems, the inner planet experiences rapid

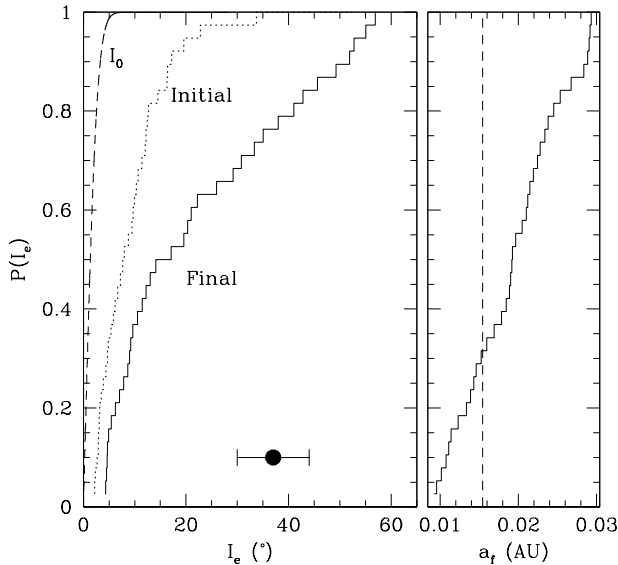


Figure 7. The right-hand panel shows the distribution of semi-major axis for the 38 systems whose evolution puts them interior to 0.03 AU. The observed location of 55 Canc e is shown as a vertical dashed line. The left-hand panel shows the final inclinations of these same systems (solid histogram). The dashed histogram is the distribution from which the initial planetary osculating inclinations were drawn. Because of secular forcing, the actual initial proper inclinations are larger, and are shown by the dotted histogram. The solid point with error bars indicates the inclination of 55 Canc d measured by McArthur et al. (2004), relative to an edge-on orbit, such as that of 55 Canc e.

eccentricity growth, to the point that it rises to a catastrophic level before tides even play a role. This is likely due to the additional forcing discussed in appendix C due to the 3:1 resonance between 55 Canc b and c.

Figures 9 and 10 show two examples of the kind of evolution that might produce a misaligned 55 Canc e. In Figure 9 we show an evolution from 0.033 AU which follows the path predicted by classical secular theory, in which a steady inward migration is punctuated with sudden jumps in eccentricity and inclination substantially in excess of the normal secular oscillations, resulting in a final inclination of almost 60° with respect to the original orbital plane. Figure 10 shows the evolution in the case where the eccentricity is pumped up to large values even at a starting location of 0.045 AU, which then drives tidal migration and again excites inclination as it passes through the unshifted inclination resonance.

3.3 Effect of the Companion

The presence of an M-dwarf companion at > 1000 AU can, in principle, induce precession of the planetary system (Innanen et al. 1997; Kaib et al. 2011; Boue' & Fabrycky 2014) if the orbit is sufficiently eccentric and inclined. However, the precession timescales are long compared to the time it takes 55 Canc e to cross the resonance, and so the orbit tilting discussed here is insensitive to the influence of the external companion. We have verified this by repeating five

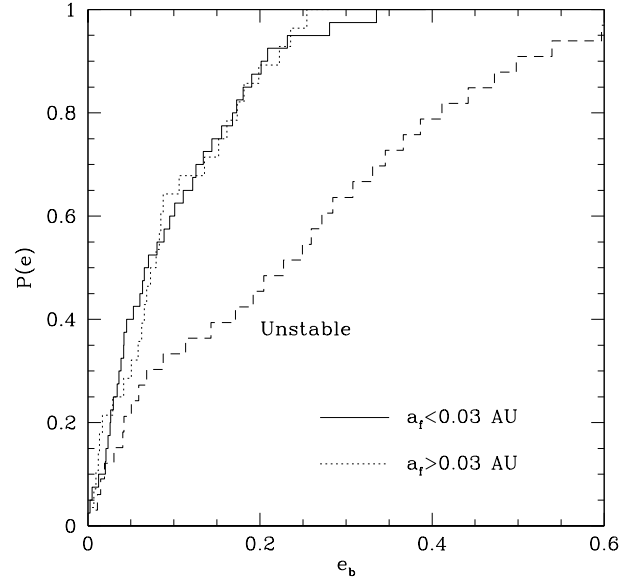


Figure 8. The solid histogram shows the initial eccentricity of planet 55 Canc b in the case where the planet e evolves to semi-major axis < 0.03 AU within 1 Myr. The dotted histogram shows the initial eccentricity in the case where the system remains stable but does not satisfy this criterion. The dashed histogram shows the initial conditions that lead to dynamical instability and shows that eccentricities > 0.25 for planet b usually lead to instability. The similarity of the dotted and solid histograms suggest that it is not simply a question of secular amplitudes that determines the tidal evolution of the system. These distributions are consistent with a Gaussian distribution of eccentricities with dispersion = 0.12.

of the simulations which crossed the resonance but including a $0.26M_\odot$ companion with semi-major axis 1250 AU, eccentricity = 0.93 and inclination 115° as discussed by Kaib et al. (2011). In all cases the eccentricity and inclination excitation was reproduced, with rapid eccentricity pumping followed by circulation, and the final orbital tilt of 55 Canc e relative to the other planets.

4 RESULTS

Our principal goal in this paper is to examine the effect of secular interactions coupled with tidal evolution on the configuration of the 55 Cancri planetary system. The generic behaviour of multi-planet systems under the influence of tidal evolution is that the eccentricities of several planets can be reduced, while the bulk of the semi-major axis evolution is borne by the innermost planet (Wu & Goldreich 2002; Greenberg & van Laerhoven 2011; Hansen & Murray 2014). Such behaviour in this system would imply that 55 Canc e began with a larger semi-major axis and migrated to the one observed today.

If 55 Canc e began with a semi-major axis > 0.033 AU, it will have crossed multiple secular resonances, dominated by the pair of planets 55 Canc b and 55 Canc c, which could have excited both substantial eccentricities and inclinations. We have demonstrated these effects using both classical sec-

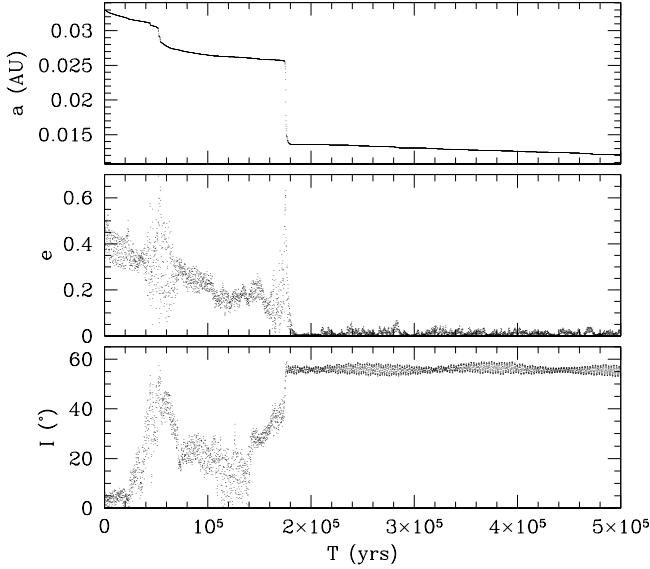


Figure 9. The upper panel shows the evolution of the semi-major axis, the middle panel the evolution of the eccentricity, and the lower panel the evolution of the inclination. The case shown here proceeds along the normal evolutionary path, with both eccentricity and inclination resonances occurring near 0.03 AU.

ular theory, analytic estimates and direct numerical integrations. These suggest that inclinations of $30 - 40^\circ$ between 55 Canc e and the other planets in the system are quite possible for initial conditions that draw planetary eccentricities from a Gaussian with dispersion $\sigma_e = 0.12$ (an approximate fit to the dynamically stable portion of our simulations – see Figure 8) and mutual inclinations from a Gaussian distribution with a $\sigma_i = 2^\circ$ dispersion (consistent with the flat planetary systems observed by the Kepler satellite). The substantial amplification is a consequence of the large mass ratio between 55 Canc e and 55 Canc b, which causes any coupling between the planets to be reflected disproportionately in the smaller of the pair. The median eccentricity of the input planets, once the dynamically unstable systems are removed, is ~ 0.07 , which is similar to the value expected for a five planet system (~ 0.085) from the power law fit of Limbach & Turner (2014).

The ability to generate a substantial inclination offset from the orbital plane of the original planetary system offers an explanation for the tension between the astrometric measurement of 55 Canc d’s inclination by McArthur et al. (2004) and the transitting nature of 55 Canc e (Winn et al. 2011; Demory et al. 2011). One observation potentially in conflict with this scenario is the statistically marginal detection of an extended H atmosphere of 55 Canc b by Ehrenreich et al. (2012). If confirmed, this would suggest a different configuration for the system, with an approximate alignment of 55 Canc e and b.

4.1 Planetary Heating

The passage through the eccentricity resonance causes a rapid increase in the eccentricity of 55 Canc e and a cor-

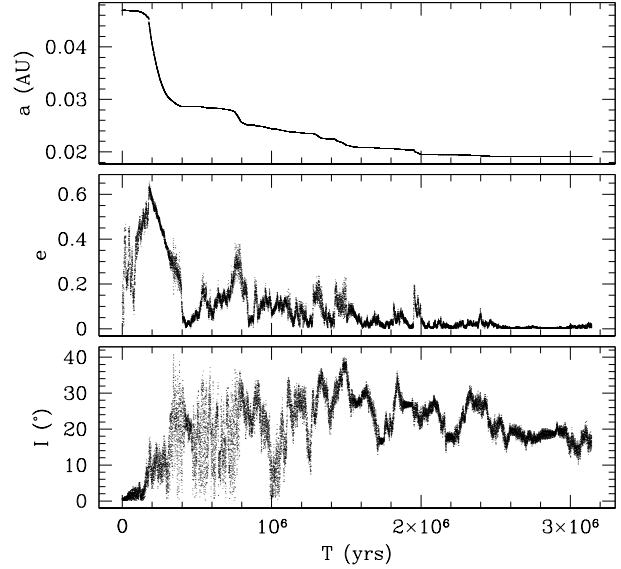


Figure 10. The upper panel shows the evolution of the semi-major axis, the middle panel the evolution of the eccentricity, and the lower panel the evolution of the inclination. In this case, the eccentricity resonance is shifted outwards, to ~ 0.043 AU.

responding rapid decrease in the periastron distance. The strong radial dependance of the tidal force means that this leads to a sharp increase in the rate of tidal dissipation and tidal heating, which in turn may substantially influence the structure of the planet. In particular, we note that the amount of energy available could potentially have removed a substantial amount of Hydrogen from 55 Canc e.

To estimate the impact of the heating on the structure of the putative planet, we note that the final planetary semi-major axis is roughly half that of the secular resonance, so that the binding energy dissipated as a result of the resonance crossing is $> 10^{42}$ ergs. This is comparable to the gravitational binding energy of a Neptune mass planet, and so can substantially influence the structure of the planet.

The 55 Cancri system already contains several planets, such as 55 Canc c and 55 Canc f, which have masses similar to Neptune or Uranus. Thus, 55 Canc e may potentially represent the rocky core of a thermally altered version of this class of planet. To ascertain the likelihood of this, we consider initial parameters for 55 Canc e, of a mass of $20M_\oplus$ and a radius of $4R_\oplus$. The rate at which this energy is dissipated will depend on the rate of tidal dissipation, which we take to be characterised by $Q' \sim 10^4$, as in the case of Neptune (Banfield & Murray 1992; Zhang & Hamilton 2008). Assuming an average eccentricity ~ 0.5 during this period, and the constant time-lag model (Hut 1981) for tidal dissipation, we find that the binding energy is dissipated over a period $\sim 10^6$ years, yielding an average luminosity $\sim 10^{-4}L_\odot$.

The effective temperature of a $4R_\oplus$ planet, radiating at $10^{-4}L_\odot$, is $\sim 3000\text{K}$, comparable to the hottest estimated equilibrium temperatures of irradiated giant planets (e.g. Konacki et al. 2003; Hebb et al. 2009; Gillon et al. 2014), and $\sim 40\%$ larger than the equilibrium temperature maintained by irradiation for this planet. Nevertheless, as in the case

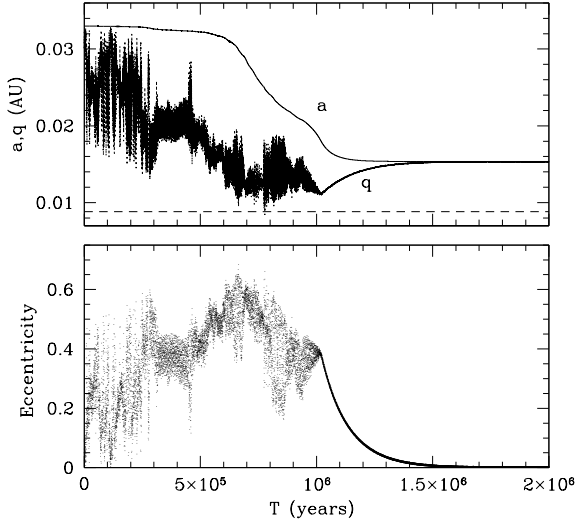


Figure 11. The upper panel shows the evolution of both the semi-major axis (upper, smooth, curve) and the periastron (lower curve) for a $20M_{\oplus}$ planet driven to high eccentricity by the crossing of a secular resonance. The horizontal dashed line indicates the semi-major axis at which a $20M_{\oplus}$, $4R_{\oplus}$ planet will fill its Roche lobe. The lower panel shows the corresponding eccentricity excitation.

of hot Jupiters on these scales, mass loss by Jeans escape is still not sufficient to substantially alter the planet mass, because $\lambda \sim GMm_p/RkT \sim 12$ for such a planet with this effective temperature.

However, dissipation does not only increase the temperature of the planet. We have previously reviewed the impact of strong tidal heating on gaseous giant planets (Hansen 2012) and found that the principal repository of the energy at high levels of dissipation is in the binding energy of the planet (i.e. at the level of dissipation relevant here, the radius of the planet increases, and central temperature can even drop). For the parameters of relevance here, the radius need only expand to $\sim 6.5R_{\oplus}$ to begin Roche lobe overflow at periastron and initiate mass loss.

To demonstrate this, we have repeated one of our simulations but replaced 55 Canc e with a $20M_{\oplus}$ object, and adjusted the level of dissipation to mimic a value of $Q' \sim 10^4$ as appropriate for Neptune. Assuming that the radius of the planet is now $4R_{\oplus}$, this requires weakening the numerical dissipation by only a factor of 60, because Q' scales with the fifth power of the planetary radius. The resulting evolution is shown in Figure 11. We see that the character of the evolution is the same, with excitation to high value of eccentricity and a sharp drop in semi-major axis, although a little less steep, as befits the weaker dissipation. We also show the evolution of the periastron during this period and note that it skirts the edge of Roche-lobe overflow even for an un-inflated radius of $4R_{\oplus}$. Thus, even a small amount of radius inflation due to the tidal dissipation will drive this planet into a mass loss event.

Thus, it is possible that the present mass and radius

of 55 Canc e are the result of mass loss, probably through Roche lobe overflow, induced by the strong tidal heating generated by the passage through the secular eccentricity resonance. If this is the case, 55 Canc e may originally have been a Neptune-mass planet, more similar to other known members of the system, such as 55 Canc c and 55 Canc f, suggesting migration as a chain of giant planets and failed cores. Residual heating may still make a contribution to the amplitude of the secondary eclipse (Bolmont et al. 2013) if the eccentricity is in the range $\sim 0.001 - 0.01$.

4.2 Other Systems

The results above suggest that the 55 Cancri system may exhibit a substantial inclination dispersion, but this is also a relatively unusual planetary system, as most short period Jupiters do not reside in systems of non-hierarchical high multiplicity (Wright et al. 2009; Steffen et al. 2012). Thus, it is of interest to enquire as to the frequency of such secular resonances in compact planetary systems. Table 2 shows examples of several systems which may possess such a resonance.

For systems detected via radial velocities, we examine those systems which possess three or more planets inside 0.5 AU, at least two of which lie outside 0.05 AU. In addition to 55 Cancri, this yields 61 Vir (Vogt et al. 2010), HD 40307 (Mayor et al. 2009) and HD 10180 (Lovis et al. 2011) around solar-type stars, and GJ 876 (Rivera et al. 2010) around an M star. In each case, we consider the secular architecture of the system given the nominal semi-major axes and masses, and examine how this changes as we vary the semi-major axis of the innermost planet. This accounts for possible motion due to tidal evolution, which is reflected primarily in the evolution of the innermost planet for secularly coupled systems (Hansen & Murray 2014). However, some care is necessary as several of these systems contain uncertain detections. For HD 40307, we have adopted the more conservative configuration because the more uncertain planets (Tuomi et al. 2013) reside further out and including them turns out to not significantly change the results. In the case of HD 10180, we include the uncertain innermost planet as a potential analogue to 55 Canc e. We note also that more strongly resonant systems, like GJ 876, may exhibit more complicated behaviour due to untreated resonant effects.

With these caveats, we find that each of the examined systems possess at least one secular resonance in both inclination and eccentricity in the region through which a planet would pass due to tidal evolution. In some cases, such as the 61 Vir and HD 10180 systems, the inner planet would appear to actually be near the location of a secular resonance at present, offering a potential explanation for non-zero eccentricities despite proximity to the star yielding strong tidal effects.

In the case of systems detected via transits, passage through an inclination resonance is likely to prevent a planet from being observed in transit, assuming the natal planetary system is edge-on in the first place. Such excitations may explain inner holes in otherwise densely packed systems observed by Kepler. An example is the Kepler-11 system (Lissauer et al. 2011b), which shows 6 planets, five of which are between 0.09–0.3 AU, but none interior to 0.09 AU.

Table 2. Orbital periods of possible secular resonances in exoplanetary systems, where P_e indicates eccentricity resonances and P_i indicates inclination resonances. Numbers in parentheses are caused by first order mean motion resonances. The final column for the RV planets shows the observed orbital period of the currently known exoplanet.

System	P_e (days)	P_i (days)	P (days)
RV Systems, assuming inner planet migration			
ρ 55 Cancri	1.66	2.0	0.74
GJ 876	7.1, (14.7)	7.3, 9.8, 17.0	1.9
61 Vir	4.2, (18.5)	6.8	4.2
HD 40307b	0.9, (4.7)	2.2, 3.9	4.2
HD 10180	1.2, (3.0)	0.8, 1.6	1.2
Transiting Systems, assuming an undetected $1M_{\oplus}$ inner planet			
KOI-94	0.9, (1.87) & 2.1	1.2 & 2.1	
Kepler-11	2.4, (5.1), 8.0	1.3, 6.1, 8.0	
Kepler-30	(13.9), 14.8	14.8	
Kepler-9	1.0, 2.5	7.5	
Kepler-51	

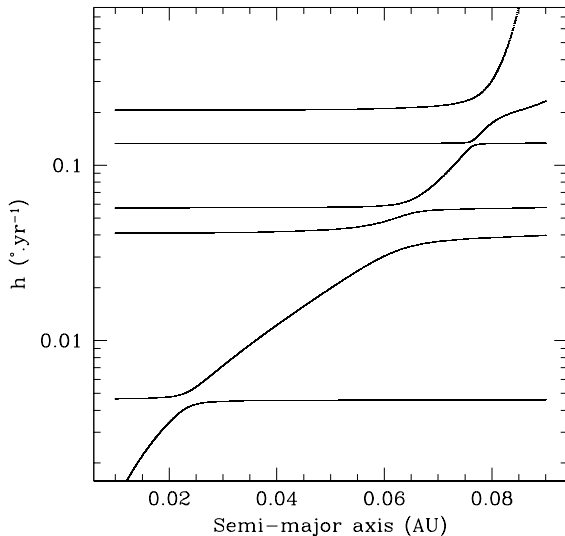


Figure 12. The curves show the change in the secular inclination eigenfrequencies of a hypothetical planetary system constructed by adding an interior $1M_{\oplus}$ planet to the known planetary system Kepler-11. As the semi-major axis of the additional planet is varied, we see that there is an avoided crossing at ~ 0.065 AU.

If we examine the secular architecture of this system assuming the presence of a seventh, $1M_{\oplus}$ planet located in the interior hole¹, we find avoided crossings in both eccentricity and inclination near semi-major axes ~ 0.065 AU, and other secular inclination resonances at 0.0233 AU and 0.0763 AU. Thus, it is possible that Kepler-11 contains a

low mass planet in the observed inner ‘hole’, but which is inclined relative to the outer planets. The inclination could be substantial if the current period is < 8 days. The Kepler planet sample contains a large number of multiple planet systems with potential for secular resonances. KOI-94 (Weiss et al. 2013) is interesting because of the presence of a Saturn mass planet in a similar orbit to 55 Cancri. The innermost planet lies just outside a pair of secular resonances at 3.0 days (eccentricity) and 3.4 days (inclination) and so is consistent with a lack of inclination excitation. If we allow for the existence of a $1M_{\oplus}$ planet interior to this, eccentricity resonances are found at 0.9 and 2.1 days (and a mean motion resonance at 1.9 days) and inclination resonances at 1.2 and 2.1 days. Thus, a planet that has tidally migrated to orbital periods < 2 days in this system could have had its inclination pumped up and have avoided transit. Another compact multiplanet system containing a massive planet is Kepler-30 (Fabrycky et al. 2012). However, the only resonances encountered by a tidally migrating $1M_{\oplus}$ inner planet lie at 14.8 days (both inclination and eccentricity) and at 13.9 days (a mean motion resonance). These may be too far out to be strongly affected by tides. Kepler-9 (Holman et al. 2010), shows two Saturn-class planets and an interior low mass planet, that we will assume to be $1M_{\oplus}$ again. Since this inner planet does indeed transit, we must assume little inclination excitation has taken place in this system. Indeed, the sole inclination resonance for this configuration lies at 7.5 days, so that the planet would not experience any excitation if it started the migration interior to this point. Eccentricity resonances are found at 1.0 and 2.5 days, bracketing the observed period. Kepler-51 (Steffen et al. 2013) is an example of a compact Kepler planetary system with a large inner hole but no Jovian-class planets. In this case, an inner $1M_{\oplus}$ planet experiences no secular resonances. There is a frequency commensurability at 2.9 days, but no avoided crossing because the modes are almost completely decoupled (one is driven primarily by the relativistic precession).

These results are necessarily incomplete because our knowledge of the planetary systems could also be incomplete, but they illustrate the potential impact of secular res-

¹ Such a planet would yield transit timing variations of amplitude < 1 minute for Kepler-11b (Agol et al. 2005), well below the current timing accuracy (Lissauer et al. 2013), as long as it lies interior to the 2:1 mean motion resonance.

onances on the internal planetary configurations of multi-planet systems. They may be less important for lower mass systems where the precessions are weaker and relativistic effects can dominate at larger distances, but could generate substantial inclinations in the cases where Jovian-class planets are present on small scales. Alternatively, the effect of stellar spin-down from an initially rapid rotation may, in some cases, also induce secular resonant crossings, as was once proposed for the eccentricity and inclination of Mercury (Ward, Colombo & Franklin 1976).

5 CONCLUSIONS

We find that it is possible to explain the conflicting observations that 55 Canc e transits, while 55 Canc d is inclined by $\sim 53^\circ$, in terms of tidal decay of the 55 Canc e orbit that causes it to cross multiple secular resonances, which drive the planet to large eccentricities and inclinations. van Laerhoven & Greenberg (2012) have previously cast doubt on whether the system can have undergone tidal evolution because not all of the secular modes coupled to the inner planet are completely damped. However, a system need not have reached its final state of a ‘fixed point’ configuration, if the evolutionary timescale is not too short. Indeed, Hansen & Murray (2014) found many model systems which were only partially damped, and the large amplitude librations about secular alignment found by Nelson et al. are characteristic of this stage of evolution. Furthermore, it worth noting that the updated parameters of Nelson et al. do differ in important ways from the solutions analysed by van Laerhoven & Greenberg (2012). The pericenter alignment of the outer, decoupled, pair of planets, which appeared to be coincidental, is no longer supported by the data. The remaining eccentricity of 55 Canc c suggests that this system is indeed still capable of further tidal evolution, although the presence of a tentative signal (Nelson et al. 2014) between planets 55 Canc c and 55 Canc f may hint at additional influences that can masquerade as an eccentricity.

The evolution through secular resonance increases the eccentricity as well as the inclination for this planet, and can result in a substantial amount of heating within 55 Canc e. This has potentially important consequences for the use of 55 Canc e as one of the highest signal-to-noise examples of a super-Earth planet. We have shown that it is possible that 55 Canc e could have lost mass through Roche lobe overflow if it expanded due to tidal heating, and so 55 Canc e may represent a class of disrupted planetary cores that have been occasionally invoked by several authors (Gu, Lin & Bodenheimer 2003; Jackson, Barnes & Greenberg 2009; Hansen 2012; Valsecchi, Rasio & Steffen 2014), rather than a rocky planet that assembled through planetesimal collisions. A more massive and volatile-rich initial mass would make 55 Canc e comparable with the other sub-jovian planets in the system, and suggests a scenario in which 55 Canc b migrated inwards with a retinue of Neptune-mass attendants, one of which was subsequently heated and stripped to the planetary core we observe day.

We have also shown that many compact multiple planet systems exhibit possible secular resonances interior to 0.1 AU, suggesting that the phenomenon of moderate-to-highly inclined inner planets may be quite common. Such

inclination pumping could potentially explain the observed lower deficit of multiple transiting planets at very short periods in the Kepler sample (Steffen & Farr 2013). Similarly, pumping of eccentricity and subsequent tidal circulation is a potential mechanism for moving planets to very short orbital periods and promoting their disintegration (Rappaport et al. 2012, 2014; Jackson et al. 2013).

The analysis presented here is predicated on the HST astrometric detection by McArthur et al. (2004), which places some constraints but is based on a limited data span. Further astrometric observations of this system, either with the HST Fine Guidance sensor or the GAIA spacecraft, would provide a welcome improvement on this constraint, and could help to refine the parameters. A substantial mutual inclination between 55 Canc e and the rest of the planets could also be tested with transit monitoring, to search for precession of the orbit.

This research has made use of NASA’s Astrophysics Data System and of the the NASA Exoplanet Archive, which is operated by the California Institute of Technology, under contract with the National Aeronautics and Space Administration under the Exoplanet Exploration Program. The authors also acknowledge the contributions from a useful referee report.

REFERENCES

- Adams, F. C. & Laughlin, G. G., 2006a, *ApJ*, 649, 1004
- Agol, E., Steffen, J., Sari, R. & Clarkson, W., 2005, *MNRAS*, 359, 567
- Banfield, D. & Murray, N., 1992, *Icarus*, 99, 390
- Batygin, K. & Laughlin, G., 2008, *ApJ*, 683, 1207
- Bolmont, E. et al., 2013, *A&A*, 556, 17
- Boue, G. & Fabrycky, D. C., 2014, *ApJ*, 789, 111
- Bourier, V. & Hebrard, G., 2014, *A&A*, 569, A65
- Butler, R. P., Marcy, G. W., Williams, E., Hauser, H. & Shirts, P., 1997, *ApJ*, 474, L115
- Chambers, J. E., 1999, *MNRAS*, 304, 793
- Dawson, R. I. & Fabrycky, D. C., 2010, *ApJ*, 722, 937
- Demory, B.-O., et al., 2011, *A&A*, 533, A114
- Demory, B.-O., et al., 2012, *ApJ*, 751, L28
- Eggleton, P. P., Kiseleva, L. G. & Hut, P., 1998, *ApJ*, 499, 853
- Ehrenreich, D., et al., 2012, *A&A*, 547, 18
- Endl, M. et al., 2012, *ApJ*, 759, 19
- Fabrycky, D. C. et al., 2012, *ApJ*, 750, 114
- Fabrycky, D. C. et al., 2014, *ApJ*, 790, 146
- Fang, J. & Margot, J.-L., 2012, *ApJ*, 761, 92
- Fischer, D. A., et al., 2008, *ApJ*, 675, 790
- Gillon, M. et al., 2012, *A&A*, 539, 28
- Gillon, M., et al., 2014, *A&A*, 562, L3
- Goldreich, P. & Soter, S., 1966, *Icarus*, 5, 375
- Greenberg, R. & van Laerhoven, C., 2011, *ApJ*, 733, 8
- Gu, P.-G., Lin, D. N. C. & Bodenheimer, P. H., 2003, *ApJ*, 588, 509
- Hansen, B., 2010, *ApJ*, 723, 285
- Hansen, B., 2012, *ApJ*, 757, 6
- Hansen, B. & Murray, N., *MNRAS*, arXiv:1405.2342
- Hebb, L. et al., 2009, *ApJ*, 693, 1920
- Holman, M. J. et al., 2010, *Science*, 330, 51
- Hut, P., 1981, *A&A*, 99, 126
- Innanen, K. A., Zheng, J. Q., Mikkola, S. & Valtonen, M. J., 1997, *AJ*, 113, 1915
- Jackson, B., Barnes, R. & Greenberg, R., 2009, *ApJ*, 698, 1357
- Jackson, B., Greenberg, R. & Barnes, R., 2008, *ApJ*, 681, 1631

- Jackson, B., et al., 2013, ApJ, 779, 165
 Kaib, N. A., Raymond, S. N. & Duncan, M. J., 2011, ApJ, 742, L24
 Kipping, D. M., 2013, MNRAS, 434, L51
 Konacki, M., Torres, G., Jha, S. & Sasselov, D. D., 2003, Nature, 421, 507
 Laskar, J., 1994, A&A, 287, L9
 Laskar, J. & Gastineau, M., 2009, Nature, 459, 817
 Limbach, M. E. & Turner, E. L., 2014, arXiv:1404.2552
 Lissauer, J. J., et al., 2011a, ApJS, 197, 8
 Lissauer, J. J., et al., 2011b, Nature, 470, 53
 Lissauer, J. J. et al., 2013, ApJ, 770, 131
 Lopez-Morales, M., et al., 2014, ApJ, 792, L31
 Lovis, C., et al., 2011, A&A, 528, 112
 Malhotra, R., Fox, K., Murray, C. D. & Nicholson, P. D., 1989, A&A, 221, 348
 Marcy, G. W. et al., 2002, ApJ, 581, 1375
 Mardling, R. A. & Lin, D. N. C., 2004, ApJ, 614, 955
 Mayor, M., et al., 2009, A&A, 493, 639
 McArthur, B. E. et al., 2004, ApJ, 614, L81
 Minton, D. A. & Malhotra, R., 2011, ApJ, 732, 53
 Mugrauer, M., Neuhauser, R., Mazeh, T., Guenther, E., Fernandez, M. & Broeg, C., (2006) AN, 327, 321
 Murray, C. D. & Dermott, S. F., 1999, Solar System Dynamics, Cambridge University Press, Cambridge
 Nelson, B. E. et al., 2014, MNRAS, 441, 442
 Rappaport, S., et al., 2012, ApJ, 752, 1
 Rappaport, S. et al., 2014, ApJ, 784, 40
 Rivera, E. et al., 2010, ApJ, 719, 890
 Saha, P. & Tremaine, S., 1994, AJ, 108, 1962
 Seager, S., Kuchner, M., Hier-Majumder, C. A. & Militzer, B., 2007, ApJ, 669, 1279
 Shen, Y. & Turner, E. L., 2008, ApJ, 685, 553
 Steffen, J. H. et al., 2012, Proc. Nat. Acad. Sci., 109, 7928
 Steffen, J. H., et al., 2013, MNRAS, 428, 1077
 Steffen, J. H. & Farr, W. M., 2013, ApJ, 774, L12
 Tremaine, S. & Dong, S., 2012, ApJ, 143, 94
 Tuomi, M., Anglada-Escude, G., Gerlach, E., Jones, H. R. A., Reiners, A., Rivera, E. J., Vogt, S. S. & Butler, R. P., 2013, A&A, 549, 48
 Valsecchi, F., Rasio, F. A. & Steffen, J. H., 2014, ApJ, 793, L3
 van Laerhoven, C. & Greenberg, R., 2012, Cel. Mech. Dyn. Astron., 113, 215
 Vogt, S. S., et al., 2010, ApJ, 708, 1366
 Wang, J. & Ford, E. B., 2011, MNRAS, 418, 1822
 Ward, W. R., Colombo, G. & Franklin, F. A., 1976, Icarus, 28, 441
 Weiss, L. M. et al., 2013, ApJ, 768, 14
 Winn, J. N., et al., 2011, ApJ, 737, L18
 Wright, J. T., Upadhyay, S., Marcy, G. W., Fischer, D. A., Ford, E. B. & Johnson, J. A., 2009, ApJ, 694, 1084
 Wu, Y. & Goldreich, P., 2002, ApJ, 564, 1024
 Zhang, K. & Hamilton, D. P., 2008, Icarus, 193, 267

APPENDIX A: ECCENTRICITY AND INCLINATION EXCITATION DUE TO SECULAR RESONANCE CROSSING

We consider an extended version of the Hamiltonian discussed in Minton & Malhotra (2011),

$$\begin{aligned} H &= H_e + H_i \\ &= -g_0 J - h_0 Z + \epsilon \sqrt{2J} \cos(\bar{\omega}_p - \bar{\omega}) + \delta \sqrt{2Z} \cos(\Omega_p - \Omega) \end{aligned} \quad (\text{A1})$$

where $J = \sqrt{a}(1 - \sqrt{1 - e^2})$, $Z = \sqrt{a(1 - e^2)}(1 - \cos i)$, g_0 and h_0 are the precession frequencies for the longitude of periastron $\bar{\omega}$, and longitude of the ascending node Ω respectively. The parameters ϵ and δ represent the strength of the coupling to the secular modes, whose orientations are represented by $\bar{\omega}_p$, and Ω_p .

We express these quantities as

$$g_0 = n \left[\frac{1}{4} \sum_j \frac{m_j}{m_c} \alpha_j^2 b_{3/2}^{(1)}(\alpha_j) + \frac{3Gm_c}{c^2 a} \right] \quad (\text{A2})$$

$$h_0 = \frac{n}{4} \sum_j \frac{m_j}{m_c} \alpha_j^2 b_{3/2}^{(1)}(\alpha_j) \quad (\text{A3})$$

$$\epsilon = \frac{n}{4} \sqrt{Gm_c a} \sum_j \frac{m_j}{m_c} \alpha_j^2 b_{3/2}^{(2)}(\alpha_j) E_j \quad (\text{A4})$$

$$\delta = \frac{n}{4} \sqrt{Gm_c a} \sum_j \frac{m_j}{m_c} \alpha_j^2 b_{3/2}^{(1)}(\alpha_j) I_j \quad (\text{A5})$$

where E_j and I_j are the eigenvector contributions from each planet to the mode under discussion, and g_0 includes the effect of relativistic precession to lowest order.

The approach of MM11 is to perform a pair of canonical transformations to variables x and y , represented by $x = \sqrt{2J} \cos \phi$ and $y = \sqrt{2J} \sin \phi$, where $\phi = \bar{\omega}_p(t) - \bar{\omega}$. In our case, it is $\bar{\omega}$, rather than $\bar{\omega}_p$, that is a function of time, but the formalism remains the same. However, we must now incorporate changes in ϵ concomitant with the changes in g_0 , since both are affected by the radial migration of the planet.

Following the formalism of MM11, we find that the Hamiltonian equations of motion yield

$$\dot{x} = \dot{g}_0 y t \quad (\text{A6})$$

$$\dot{y} = -\epsilon - (\dot{g}_0 x + \dot{\epsilon}) t \quad (\text{A7})$$

which is the same as equations (9) and (10) of MM11, except for the $\dot{\epsilon}$ term.

The method of solution is similar, whereby one can find a homogeneous solution in terms of trigonometric functions of $\dot{g}_0 t^2$, and then substitute back to find a solution to the inhomogeneous version by solving for the multiplicative constants as functions of time. Thus, we assume

$$x(t) = A(t) \cos \dot{g}_0 t^2 + B(t) \sin \dot{g}_0 t^2 \quad (\text{A8})$$

$$y(t) = -A(t) \sin \dot{g}_0 t^2 + B(t) \cos \dot{g}_0 t^2 \quad (\text{A9})$$

MM11 solved for A and B in terms of the Fresnel integrals

$$S(t) = \int_0^t \sin z^2 dz \quad (\text{A10})$$

$$C(t) = \int_0^t \cos z^2 dz. \quad (\text{A11})$$

The presence of ϵ term introduces a slight modification to the solution, yielding

$$A(t) = \frac{\epsilon}{\sqrt{|\dot{g}_0|}} S(t') + \frac{\dot{\epsilon}}{|\dot{g}_0|} S'(t') \quad (\text{A12})$$

$$B(t) = -\frac{\epsilon}{\sqrt{|\dot{g}_0|}} C(t') - \frac{\dot{\epsilon}}{|\dot{g}_0|} C'(t') \quad (\text{A13})$$

where $t' = \sqrt{|\dot{g}_0|}t$, and S' and C' are modified versions of the Fresnel integrals, such that

$$S'(t) = \int_0^t z \sin z^2 dz$$

and

$$C'(t) = \int_0^t z \cos z^2 dz.$$

For our purposes, we care primarily about the properties of the solution as t' goes from $-\infty$ to $+\infty$ (i.e. the transformation of the orbit as it passes well beyond the resonance). Thus, we can make use of the identity

$$\int_0^\infty x^m e^{ix^n} dx = \frac{1}{n} \Gamma\left(\frac{1+m}{n}\right) e^{i\pi(1+m)/2n}$$

to evaluate $S(\infty) = C(\infty) = \sqrt{\pi/8}$, $S(-t) = -S(t)$, $C(-t) = -C(t)$ (as in MM11), as well as $S'(\infty) = 1/2$, $C'(\infty) = 0$, and $S'(-t) = S'(t)$, $C'(-t) = C'(t)$. So, we find that the evenness of the functions S' and C' mean that the contributions of the ϵ term to the asymptotic behaviour average out and we recover the same result as MM11.

Thus, our final expressions are the same as those from MM11,

$$J_f = J_i + \frac{\pi\epsilon^2}{2|\dot{g}_0|} + \epsilon\sqrt{\frac{2\pi J_i}{|\dot{g}_0|}} \cos \bar{\omega}$$

with the equivalent expression for the inclination

$$Z_f = Z_i + \frac{\pi\delta^2}{2|\dot{h}_0|} + \delta\sqrt{\frac{2\pi Z_i}{|\dot{h}_0|}} \cos \Omega.$$

The expressions for ϵ and δ are as above, and the expressions for \dot{g}_0 and \dot{h}_0 are

$$\frac{dg_0}{dt} = \frac{1}{a} \frac{da}{dt} n \left[\frac{1}{8} \sum_j \frac{m_j}{m_c} \alpha_j^2 \gamma_j - \frac{15}{2} \frac{Gm_c}{c^2 a} \right], \quad (\text{A14})$$

and

$$\frac{dh_0}{dt} = \frac{1}{a} \frac{da}{dt} n \frac{1}{8} \sum_j \frac{m_j}{m_c} \alpha_j^2 \gamma_j \quad (\text{A15})$$

where $\gamma_j = b_{3/2}^{(1)} + 3\alpha_j \left[b_{5/2}^{(0)} - 2\alpha b_{5/2}^{(1)} + b_{5/2}^{(2)} \right]$.

For the 55 Cancri system, the relevant frequencies and couplings are all dominated by 55 Canc b, with contributions from 55 Canc c and relativity contributing at the one percent level. The eigenfunction for the mode that drives the excitation through the resonance actually contains a stronger contribution (see Figure 1) from 55 Canc c (by a factor ~ 5), but the greater mass and proximity of 55 Canc b means that the functions ϵ and δ still only contain a $\sim 5\%$ contribution from 55 Canc c. Thus, in our discussions, we will refer primarily to excitation by interaction with 55 Canc b.

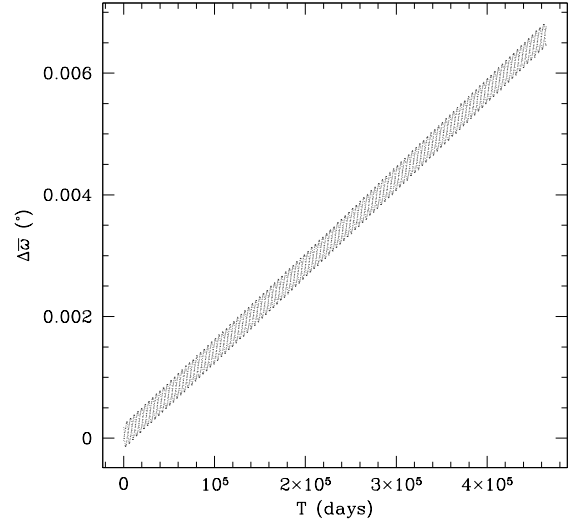


Figure B1. The points show the accumulated deviation between the numerically integrated argument of periastron and the value calculated analytically, for a planet of semi-major axis 0.05 AU, and eccentricity $e = 0.2056$. Only a single planet was included and no tidal damping was included.

APPENDIX B: CALIBRATION OF THE RELATIVISTIC PRECESSION AND NUMERICAL TIDAL DISSIPATION

The Mercury code (Chambers 1999) does not include a prescription for relativistic precession or tidal damping, so we incorporate an extra user-defined force as follows. The relativistic precession term is standard but can sometimes require special handling for proper implementation (e.g. Saha & Tremaine 1994). However, our interests are on sufficiently small scales that our timesteps are chosen small enough to properly resolve the precession anyway, and a direct implementation with the MVS symplectic algorithm yields answers of sufficient accuracy. Figure B1 shows the accumulation of the difference between the numerically calculated relativistic precession using Mercury and the expected analytic value (calculated for a single planet at 0.05 AU and with no tidal effects included). The drift of the location of periastron is $\sim 5 \times 10^{-6} \text{ } ^\circ \text{ } yr^{-1}$, well below any of the precession frequencies of interest in this system (see Figure 1).

We have previously (Hansen 2010) calibrated tidal interactions based on the constant time-lag model of Hut (1981) and Eggleton, Kiseleva & Hut (1998), and so we adopt the force law from Hut (1981). The component that damps eccentricity is that which acts to dissipate the radial component of the planetary velocity, namely

$$F = -\alpha \frac{\mathbf{r} \cdot \dot{\mathbf{r}}}{r^9}$$

where \mathbf{r} and $\dot{\mathbf{r}}$ are the heliocentric radius and radial velocity vectors. In Hut's formula, the constant $\alpha = 9GM_*^2 k \tau R_p^5$, where k is the apsidal constant, τ a timescale that encodes the strength of dissipation, and R_p is the radius of the planet (in which the tides are being dissipated). For the purposes

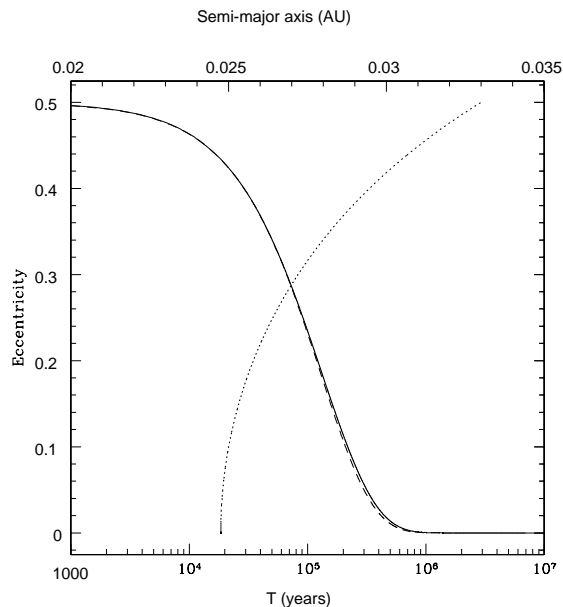


Figure B2. The solid line shows the evolution of an isolated 55 Canc e analogue, under the influence of our tidal dissipation prescription. The plot actually contains a dashed line representing $e = 0.5\exp(-t/1.3 \times 10^5 \text{ yrs})$, but it is hard to see because the fit is excellent. The dotted line relates the eccentricity to the semi-major axis, given on the upper axis, and demonstrates the conservation of angular momentum during tidal decay.

of calibrating the simulations α is a single number, whose physical relevance will depend on the relationship between the various physical quantities of which it is composed. In the low eccentricity limit, the resulting evolution of the eccentricity is an exponential damping, whose characteristic timescale is determined by α .

Figure B2 shows the evolution for a 55 Canc e analogue, begun at 0.033 AU, with eccentricity=0.5 with the same calibration for α as the simulations described in the main text. This is very well fit by an exponential decay on a timescale of 1.3×10^5 years. In the formalism of Hansen (2010), and assuming a planet of mass $8M_{\oplus}$ and radius $2R_{\oplus}$, this corresponds to $\sigma_p \sim 2.5 \times 10^{-50} g^{-1} cm^{-2} s^{-1}$. This is a considerably stronger level of bulk dissipation than found for giant planets in that paper, but such a difference is to be expected for a terrestrial-class planet, and indeed, it is only a factor of 10 larger than the nominal value used by Bolmont et al (2013), based on an extrapolation from Earth dissipation levels. If cast in terms of the traditional tidal Q , it corresponds to $Q_p = 13$, using the expression from Jackson, Greenberg & Barnes (2008), which is also comparable with an earth-like dissipation.

If we adopt a Neptune mass and radius of $20M_{\oplus}$ and $4R_{\oplus}$, this would correspond to $Q_p \sim 150$, which is a little low compared to that observed for Uranus & Neptune (Banfield & Murray 1992; Zhang & Hamilton 2008).

Figure B2 also shows the trajectory of the planet evolution in semi-major axis as a function of eccentricity. The curve traces out that expected due to the conservation of angular momentum during isolated tidal evolution. It is also worth noting that the eccentricity properly asymptotes to

zero at late times. This can be compared with the late-time behaviour shown in the full runs in Figure 9 and 10, which show some fluctuations. The fact that they do not occur here demonstrates that the effect is a real one, due to residual secular perturbations from the other planets, and not due to numerical inaccuracies.

APPENDIX C: RESONANT INTERFERENCE WITH THE SECULAR INTERACTIONS

The numerical experiments demonstrate that the planets 55 Canc b and c are close enough to the 3:1 resonance that their resonant interactions may sometimes distort the secular structure of their interactions with 55 Canc e. Figures 5 and 6 showed how this can manifest itself in the Lagrangian forcing of test particles. A more direct demonstration can be found in the Fourier decomposition of an integration of the full planetary system. We have performed a fourier transform of the time series of the eccentricity of 55 Canc b for each of the two cases shown in those figures,

$$C_k = \sum_{j=0}^{N-1} e_j e^{2\pi i j k / N} \quad (C1)$$

and calculated the power spectral density

$$P(f) = \frac{1}{N^2} [|C_k|^2 + |C_{N-k}|^2], \quad (C2)$$

for a time series with a 10 day timestep and $N = 2^{21}$.

Figure C1 shows the power spectrum $P(f)$ for the case shown in Figure 5, which conforms to the standard secular evolution we expect. The power spectrum shows the strongest power at the expected secular frequency g_1 (the time series was not long enough to capture the longer secular period) with additional power in the neighbourhood of the circulation frequency of the near resonance. There is also a minimum in the power between these two values, suggesting a clear separation between the resonant and secular phenomena.

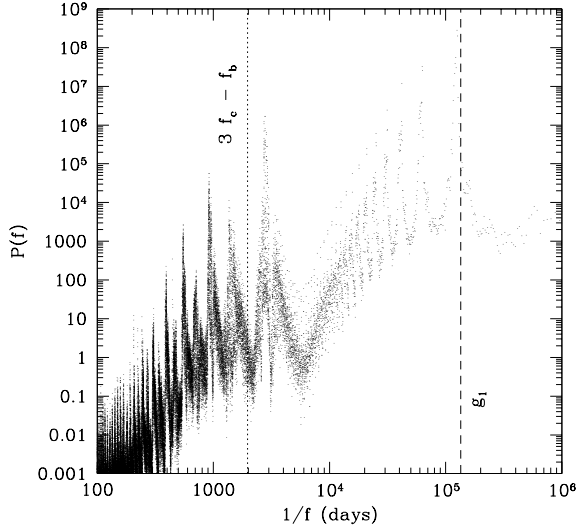
For a different set of initial eccentricities and longitudes of periastron, corresponding to Figure 6, we find the power spectrum shown in Figure C2. In this case the secular frequency is shifted to higher values relative to the classical value g_1 , and more power is found between this frequency and the higher circulation frequency, indicating a stronger interaction. The shift in frequency of the secular mode is consistent with the change in the location of the secular resonance observed in Figure 5.

Could this simply be the case of a set of initial conditions that put almost no power into the mode with frequency g_1 , rather than a shift driven by proximity to resonance? Figure C3 shows the power spectrum of a simulation run with exactly the same parameters as in the case of Figure C2, except that the semi-major axis of 55 Canc c was moved from 0.237 AU to 0.24 AU. We see that this change in 1% is sufficient to restore the mode frequency to its expected classical value, indicating that the observed change in frequency is directly linked to the proximity to resonance.

To gain a qualitative understanding of this phenomenon, let us collect the relevant secular and resonant terms, up to second order in eccentricity, for the pair

Table C1. Constants that define the averaged secular and resonant interactions of the 55 Canc b and 55 Canc c planet pair.

C_1	0.263	C_4	2.996	C_7	1.112
C_2	0.139	C_5	-6.133		
C_3	-2.149	C_6	1.197		

**Figure C1.** $P(f)$ is the power spectral density of the eccentricity of 55 Canc b, plotted against the corresponding period in the time series. The vertical dotted line shows the period associated with the expected circulation frequency $3n_c - n_b$ of the planet pair 55 Canc b and 55 Canc c. The vertical dashed line is the expected secular frequency g_1 based on classical secular perturbation theory.

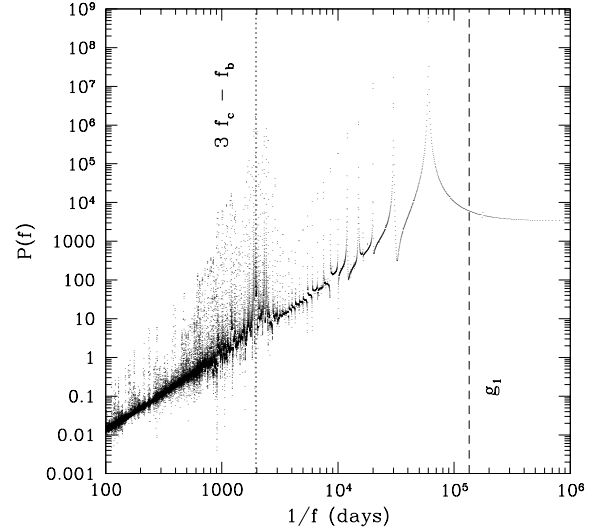
55 Canc b and 55 Canc c. The disturbing functions, averaged over short period terms, are

$$\begin{aligned} \langle R_b \rangle = & 8.73 \times 10^{-4} \left[C_0 + C_1 (e_b^2 + e_c^2) + \right. \\ & C_3 e_b e_c \cos(\bar{\omega}_c - \bar{\omega}_b) + C_4 e_b^2 \cos(\Theta - 2\bar{\omega}_b) \\ & \left. + C_5 e_b e_c \cos(\Theta - \bar{\omega}_b - \bar{\omega}_c) + C_6 e_c^2 \cos(\Theta - 2\bar{\omega}_c) \right] \end{aligned} \quad (\text{C3})$$

$$\begin{aligned} \langle R_c \rangle = & 4.133 \times 10^{-3} \left[C_0 + C_1 (e_b^2 + e_c^2) + \right. \\ & C_3 e_b e_c \cos(\bar{\omega}_c - \bar{\omega}_b) + C_4 e_b^2 \cos(\Theta - 2\bar{\omega}_b) \\ & \left. + C_5 e_b e_c \cos(\Theta - \bar{\omega}_b - \bar{\omega}_c) + C_7 e_c^2 \cos(\Theta - 2\bar{\omega}_c) \right], \end{aligned} \quad (\text{C4})$$

where the C_i are given in Table C1 and the difference between C_6 and C_7 is due to the differing contributions to the 3:1 resonance from the internal and external components of the indirect disturbing function. Far from resonance, the terms in the angle $\Theta = 3\lambda_c - \lambda_b$ will average to zero and the system will exhibit the traditional secular oscillations. However, if the secular oscillations bring the planetary eccentricities to low enough values, the resulting increase in the precession rate can sweep the system through resonance, inducing a brief libration.

We integrate the Lagrange equations based on equations (C3) and (C4) to describe the evolution of the

**Figure C2.** $P(f)$ is once again the power spectral density of the eccentricity of 55 Canc b, but now for a case in which the behaviour deviates significantly from the expectations of classical secular theory. In particular, we note that the period of the dominant secular mode is now substantially shifted from the vertical dashed line. A comparison with the structure observed in Figure C2 demonstrates that the power in the frequency range between the secular frequency and the circulation frequency is higher, indicating a stronger degree of interaction.

55 Canc b/55 Canc c system, for a set of initial conditions that showed the resonant interaction during the full numerical integration.

As Figure C4 demonstrates, the evolution that arises exhibits the characteristic oscillatory behaviour of secular evolution, with the planetary eccentricities undergoing quasi-sinusoidal oscillations with a range of frequencies. The most rapid oscillations are associated with the circulation of the resonant argument. However, we also see the occasional transient librations which act to change the phase of the oscillations and equivalently the amplitudes of the oscillations. The inset in Figure C4 shows the effect of one of these librations, which acts to essentially apply a random phase kick to the overall oscillations. Figure C5 demonstrates the nature of the deviations from simple circulation during this interaction. The four panels show a sequence of trajectories in the space $x_b = e_b \cos(\Theta - 2\bar{\omega}_b)$ and $y_b = e_b \cos(\Theta - 2\bar{\omega}_b)$. When the eccentricity gets small, the trajectory exhibits a reversal, which represents a transition to libration. A trajectory for a more lengthy integration is shown in Figure C6,

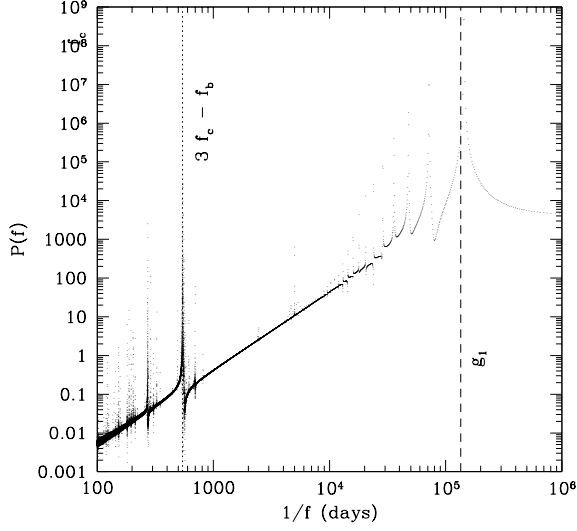


Figure C3. $P(f)$ is once again the power spectral density of the eccentricity of 55 Canc b, but now for a case in which the semi-major axis of 55 Canc c has been moved out by 1%, to reduce the effects of resonant interactions. All other parameters, including initial eccentricities and phases, are the same as in Figure C2. We see here that the distinction between the secular interactions and the circulation of the resonant angle is much clearer, and that the values correspond to the expectations of classical secular theory.

which demonstrates the presence of a critical eccentricity below which the circulation transitions to libration.

To understand this, let us extract the resonant Hamiltonian from the relevant part of $\langle R_b \rangle$, to study the dynamics of the e_b^2 resonance at low e_b . Normalising by the mass, and defining $\phi_b = \Theta - 2\bar{\omega}_b$ and $\Delta\bar{\omega} = \bar{\omega}_b - \bar{\omega}_c$, we get the Hamiltonian

$$H = [C_4 e_b^2 + C_5 e_b e_c \cos \Delta\bar{\omega} + C_6 e_c^2 \cos 2\Delta\bar{\omega}] \cos \phi_b + [C_5 e_b e_c \sin \Delta\bar{\omega} + C_6 e_c^2 \sin 2\Delta\bar{\omega}] \sin \phi_b. \quad (C5)$$

This Hamiltonian has several equilibrium points, but some are for the case when e_b and e_c are of similar magnitude, which is not our focus here. In the case when $e_b \ll e_c$ and $\bar{\omega}_b = \bar{\omega}_c$, we find two equilibrium points at $x_b = 0$ and

$$|y_b| = -\frac{e_c}{2C_4} \left(-C_5 \pm [C_5^2 - 4C_4 C_6]^{1/2} \right) = 0.217 e_c. \quad (C6)$$

This value of y_b defines a characteristic value of e_b at which the circulation of the resonant argument switches over to libration. Figure C7 shows the curves of constant H_b for the case $e_c = 0.12$ (corresponding to the value during the resonance passage shown in the inset of Figure C4), which yields the critical value of $e_b = 0.026$ (shown as a dashed circle). When the secular oscillations bring e_b below this value, the increase in secular precession sweeps the system into resonance, and the trajectory only returns to simple circulation when the oscillations bring e_b to larger values again. The behaviour is similar when the periapses are not aligned, but the locations of the equilibrium points rotate in x_b and y_b . The dramatic behaviour seen in Figures C5

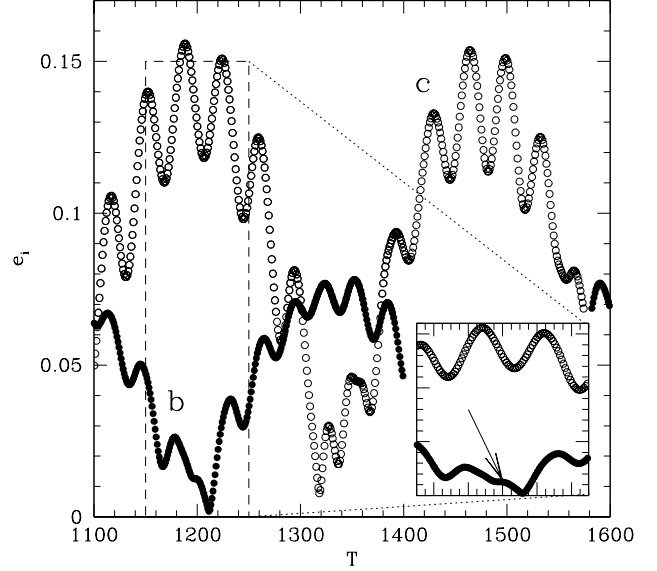


Figure C4. The solid points show the eccentricity of 55 Canc b, integrated using the Lagrange equations and disturbing functions (C3) and (C4), while the open circles show 55 Canc c. The curves show longer timescale secular oscillations allied to shorter timescale resonant oscillations. The inset shows a zoom of the passage through a brief libration in the angle $\phi = 3\lambda_c - \lambda_b - 2\bar{\omega}_b$, with the arrow indicating the time of the libration. This corresponds to a change in the phase of the secular oscillation.

and C6 are thus manifestations of the passage through the resonance as the rate of secular precession increases while e_b decreases.

Similar considerations describe the behaviour of the e_c^2 resonance, when $e_c \ll e_b$. Thus, although the nominal timescales for secular oscillations and mean motion librations are separated by almost two orders of magnitude, the excursions to low eccentricities in the secular oscillations are sufficient to enhance the precession rates to sweep the system through the resonance on an intermittent basis. The resulting interference with the secular oscillations appears to shift the frequencies sufficiently to make a measureable difference in the resonant forcing of some of our model systems. However, it appears as though this subset has less likelihood of generating observable 55 Canc e analogues, as most of the inner planets in these systems end up hitting the star (§ 3.2).

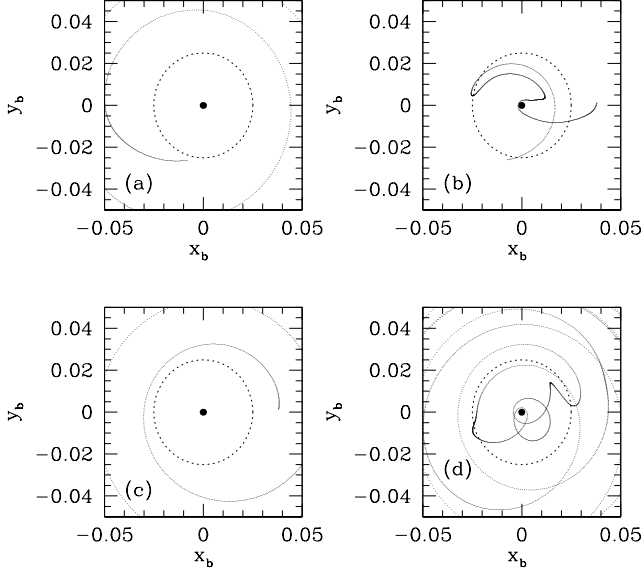


Figure C5. Panels a–d indicate a sequence of trajectories for the quantities x_b and y_b as they pass through an episode of transient libration. The particular interaction shown here is also the one responsible for the evolution during the inset in Figure C4. In particular, panel (a) covers the time 1100–1160, (b) from 1160–1230, (c) from 1230–1300 and (d) shows the evolution from here through the next interaction, i.e. from 1300–1600. The dotted circles in each panel have a radius of 0.025 and represent the critical eccentricity below which one expects an unstable equilibrium point to appear in this resonance, as discussed in the text.

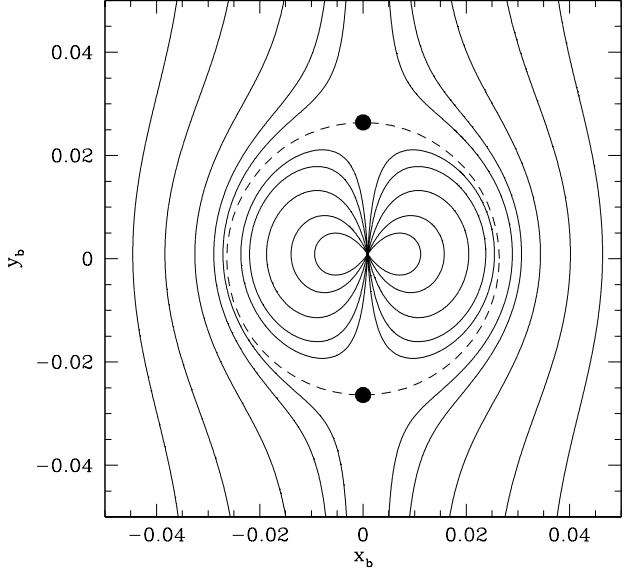


Figure C7. The curves show lines of constant H_b , based on equation (C5), for the case $e_c = 0.12$. The dashed line indicates a circle of $e_b = 0.026$. The two solid points indicate the equilibrium points on these scales. The sign of H changes upon passage through the critical e_b at fixed x_b , which drives the kinds of reversals of trajectory seen in Figure C5, because the path has to change from one side of the origin to the other.

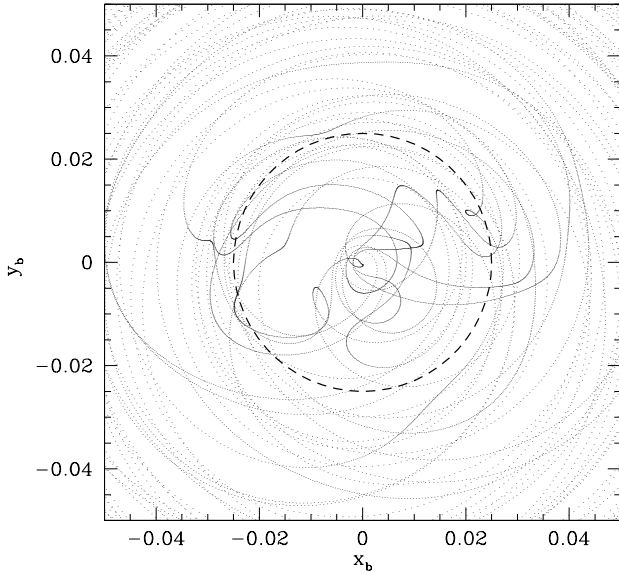


Figure C6. The heavy dashed curve represents the critical eccentricity of 0.025, and the smaller dots show the trajectory of the system evolution, which is characterised by a simple circulation exterior to this curve but by a more complicated and chaotic evolution interior to this value, as the system exhibits a resonant interaction.